ACS APPLIED MATERIALS & INTERFACES

Research Article

www.acsami.org

# Directional Superficial Photofluidization for Deterministic Shaping of Complex 3D Architectures

Seungwoo Lee,*[,†] Hong Suk Kang,[‡] Antonio Ambrosio,*[,§,∥] Jung-Ki Park,[‡] and Lorenzo Marrucci[∥]

[†]SKKU Advanced Institute of Nanotechnology (SAINT) & School of Chemical Engineering Sungkyunkwan University (SKKU), Suwon 440-746, Republic of Korea

[‡]Department of Chemical and Biomolecular Engineering and Graduate School of EEWS, Korea Advanced Institute of Science and Technology (KAIST), Daejeon 305-701, Republic of Korea

[§]School of Engineering and Applied Sciences, Harvard University, 29 Oxford Street, Cambridge, Massachusetts 02115, United States

[∥]CNR-SPIN and Dipartimento di Scienze Fisiche, Universitàdegli Studi di Napoli Federico II, Via Cintia, Napoli 80126, Italy

Supporting Information

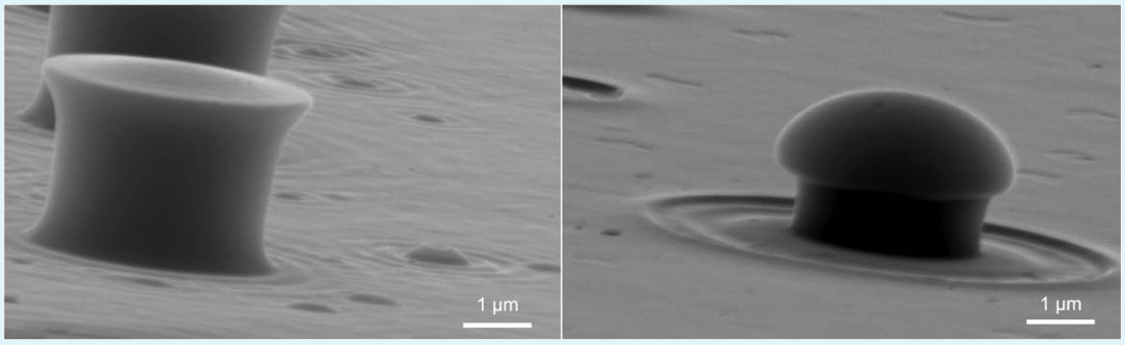


**ABSTRACT:** The fabrication of micro- and nanostructures is one of the cornerstones of current materials science and technology. There is a strong interest in processing methods capable of manufacturing engineered complex structures on a large area. A method that is gaining a growing attention in this context is based on surface reshaping of photosensitive materials, such as certain azobenzene derivatives by way of a process of light-induced mass migration, also described as "athermal photofluidization". Here, we apply this method to prestructured substrate, converting simple periodic structures initially patterned only in two dimensions into complex-shaped three-dimensional (3D) structures by a single processing step over a large area. The optical variables of the irradiating beam are used to gain unprecedented deterministic control on the resulting 3D architectures. We also provide some initial demonstrations of the potential application of this novel shaping method, including unidirectional wetting surfaces and micro- and nanoscaled fluidic channel manufactured with it.

**KEYWORDS:** *directional photofluidization, complex structures, soft matter, unidirectional wetting, fluidic channels*

## INTRODUCTION

The controlled fluidic behavior of soft matter by heat and/or electrohydrodynamic forces have led to compelling opportunities for the deterministic shaping of micro- and nanoarchitectures.[1−9] In addition to a good flexibility in controlling the structural shape, the fluidic nature, through its tendency to minimize surface energy, can significantly smooth out the surface;[5,6,10] this provides a general strategy for the reduction of the edge roughness that often limits the practical application of three-dimensional (3D) micro- and nanoarchitectures in obtaining various worthy properties.[5,6,10−13] However, such established methods for the control of fluidic behavior, while promising, have been heavily dependent on the isotropic surface tension, which offers only limited control parameters for obtaining complex structures.[1−10] Also, the intrinsic instabilities of objects fluidized by heat or other standard means have typically resulted in the lack of 3D programmability for shaping of micro- and nanoarchitectures.[1−13] Here, we show that adopting azobenzene materials (in which azobenzene molecules are incorporated into a host material)[11−21] and using light to control its fluidic-like behavior allows achieving a new degree of control in designing 3D complex soft-matter architectures.

Many azobenzene derivatives are efficient dye molecules, which absorb visible light, and exhibit *trans-cis-trans* photoisomerization cycles as a consequence of photon absorption.[11−38] A large number of these microscopic processes, in turn, can drive reorganization phenomena of the host material on a macroscopic scale, such as light-induced molecular anisotropy[39−41] and mass transfer or migration.[11−38] The latter, in particular, behaves as the material, initially solid,

Received: February 4, 2015
Accepted: March 30, 2015
Published: March 30, 2015

  

DOI: 10.1021/acsami.5b01108
ACS Appl. Mater. Interfaces 2015, 7, 8209−8217

became fluid under the effect of such light-induced molecular motions. Yet, this occurs without significant temperature variations, and hence, the name "athermal photofluidization" is sometimes used for this phenomenon.[21] This fluidic behavior, however, is quite extraordinary because the "flow", herein, is highly directional, typically parallel to the light polarization, in contrast to the heat-induced isotropic counterparts[5,6,11,13,16−19,23,26] and is spatially controlled by the light irradiation pattern in a nontrivial way.[14,16,42−48] When the irradiation stops, everything becomes "frozen" again, and hence, the reconfigured structural fidelity of azo-materials is quite stable.[11−36,42−48] Even if, all previous works has been highly limited to two-dimensional (2D) reconfiguration of pristine structures (e.g., inscription of two orthogonal gratings or 2D directional photofluidic reconfiguration of a micron scaled, simple line shape into a ellipsoidal hole with nanoscale),[11−38,42−48] such synergistic properties can make the photofluidization highly amendable to a deterministic 3D shaping of architectures in an unprecedented way.

In the present work, we exploit the light-induced mass migration phenomenon in a three-dimensionally controlled fashion and completely generalize a platform for deterministic 3D shaping of micro- and nanoarchitectures by using directional "superficial" photofluidization of azobenzene materials. As a proof of its principle, we start with a pristine structure—a regular array of microscaled cylinders—and reshape it by applying a uniform illumination, as obtained with a polarized plane wave at normal or oblique incidence. The resulting pattern is still periodic, but each unit of the pattern has acquired a 3D complex shape that is determined and precisely controlled by the light irradiation conditions and parameters, for example, the incidence angle, polarization, and the presence or absence of a capping layer on top of the cylinder array. Shapes resembling domes, mushrooms, lemons, and canoes can be achieved and fine-tuned in their 3D orientation. Furthermore, when starting with submicron-scaled PDO3 architectures, 3D shaping process in submicron scale is also available by our approach. Such 3D structures are either impossible or very difficult to obtain by other methods, particularly on a large area, so we anticipate that our approach will extend an important direction of the current toolbox of established fluidic 3D shaping methods. We also demonstrate a first simplified phenomenological modeling of the reshaping process. The new degree of flexibility and control in the design and fabrication of 3D micro- and nanoarchitectures provided by our current approach could pave the way to a number of possible applications. We present here two representative examples: (1) surfaces having controlled anisotropic wetting properties and (2) engineered micro/nanofluidic channels for biomolecular applications. Therefore, we believe that our work can provide a novel platform for a significant extension of the currently available 2D photofluidization to building custom 3D architectures over the large area.

## EXPERIMENTAL SECTION

**Preparation of Poly(disperse orange 3) (PDO3).** PDO3 (Figure S1, Supporting Information) was synthesized by condensation reaction between disperse orange 3 (Sigma-Aldrich) and bisphenol A diglycidyl ether (Sigma-Aldrich) at 120 °C for 2 days;[11,13] then, purified by nonsolvent sedimentation and subsequent vacuum-filtration. The synthesized PDO3 showed molecular weight ($M_w$) of ~4700 g/mol, polydispersity index (PDI) of 1.74, and glass transition temperature ($T_g$) of 120 °C. The absorption spectrum of the synthesized PDO3 is presented in Figure S2, Supporting Information.

**Preparation of Polydimethylsiloxane (PDMS) Stamp and Capping Layer.** We first made a mixture of PDMS solution (10 parts by weight of PDMS precursor and 1 part by weight of curing agent (Sylgard 184, Dow Corning, Midland, MI)) in a weighing cup, and subsequently degassed the mixture in vacuum desiccator for 1 h. The degassed mixture of PDMS was then carefully poured onto the prepared silicon master pattern; the silicon master pattern had already been surface treated by tridecafluoro-1,1,2,2-tetrahydrooctyl-1-trichlorosilane to reduce the surface energy. After being fully cured (at 80 °C in an oven for 1 h), the PDMS stamp was peeled from the silicon master pattern. The PDMS capping layer was molded within the flat Petri dish (the ratio of base to curing agent was 0.2 by weight ratio); the flat surface of PDMS capping layer was conformably attached on the pristine array by nonspecific van der Waals interaction.

**Molding Process for the Fabrication of Pristine PDO3 Arrays.** The pristine PDO3 array was developed by soft imprinting of PDO3 solution (dissolved in *N*-methyl-2-pyrrolidone (NMP, Sigma-Aldrich) by 10 wt %:[23,49] the droplet of PDO3 solution was carefully dropped onto glass slides; then, a prepared PDMS stamp was gently placed onto the PDO3 solution. When the solvent (i.e., NMP) was completely evaporated (12 h in 45 °C), a replicated PDO3 pattern arrays were uniformly generated. All this soft imprinting process was made by using the custom-built translational stage to ensure the process reliability.[50] The soft imprinting process left a 200 nm thick residual backing layer between the posts and substrate.

**Structural Characterizations.** The structural features of the pristine and reshaped PDO3 arrays were detailed by using scanning electrom microscopy (SEM, FEI, Sirion), optical microscope (Olympus, BX51), and atomic force microscope (Park system, XE7). The fluorescence images were obtained by using fluorescence microscope (Nikon TE2000).

**Laser Setup for Light Illumination.** Detailed scheme of laser setup for light illumination is presented in Figure S3, Supporting Information. The 532 nm wavelength laser (diode pump solid-state, Melles Griot) with intensity of 30 mW/cm$^2$ was collimated and spatially filtered, while its polarization was precisely tuned by using half- or quarter-waveplate. The laser beam intensity was controlled by neutral-density filter (ND filter); the diameter of laser beam was adjusted by iris. The final intensity of the collimated light was 10 mW/cm$^2$; this light intensity was constantly used across all the samples, except in the case of Figure 6a−c. In the case of the results in Figure 6a−c, we used initial Gaussian beam without light collimation with intensity of 30 mW/cm$^2$.

**Finite-Difference, Time-Domain (FDTD) Simulation.** The absorption characteristics of PDO3 post was detailed by numerical simulation (FDTD with home-built code) of structural unit cell with the periodic boundary conditions. A fine-grid (at least 20 points per wavelength in all directions) was constructed; a relatively long time-transient response (at least 1.5 ps) was collected for the reduction of error rate. The complex dielectric constant of PDO3 was empirically measured by the ellipsometry.[49] The spatial distribution of the minimum light intensity ($|E^2|$) within the structure was further fitted by the empirically measured threshold intensity (5 $\mu$W/cm$^2$) for inducing photofluidization.[23]

## RESULTS AND DISCUSSION

The pristine structures for our experiments are arrays of cylindrical posts made of poly(disperse orange 3) (PDO3; Figure S1, Supporting Information). We used PDO3 just as a typical representative of this class of light-sensitive azobenzene materials. It is well established that a very similar light-driven material displacement takes place in almost all azobenzene-containing glass polymers, as well as in many liquid crystalline polymers and other azobenzene materials.[11−38] Furthermore, the azobenzene materials with the specific structures could be converted into other materials, for example, by replication process.[42] The absorption spectrum of PDO3 is presented in Figure S2, Supporting Information. The samples were


DOI: 10.1021/acsami.5b01108
ACS Appl. Mater. Interfaces 2015, 7, 8209−8217

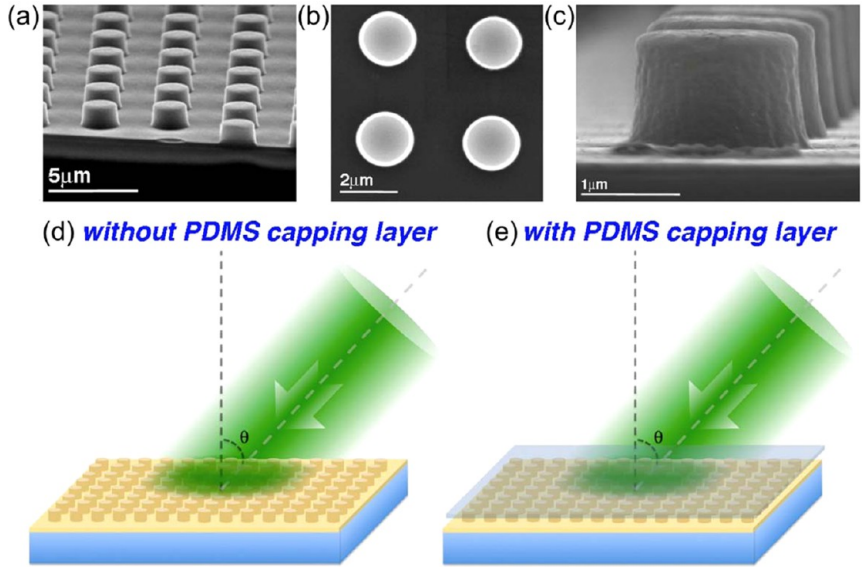


**Figure 1.** (a) SEM image of azo-PDO3 posts produced by means of soft-imprinting with a PDMS stamp. Each post is 2 $\mu$m in diameter and 1.6 $\mu$m high. The periodicity is of 4 $\mu$m. (b) SEM top view of four of the posts shown in image a. (c) Magnified image of the posts shown in image a. (d and e) Sketch of the illumination schemes. An expanded laser beam is incident on the sample surface. The incident angle $\theta$ can be varied from 0 to 60°. The direction of the incidence is represented by the white arrow inside the beam. Experimental configuration (d) without and (e) with a PDMS capping layer.

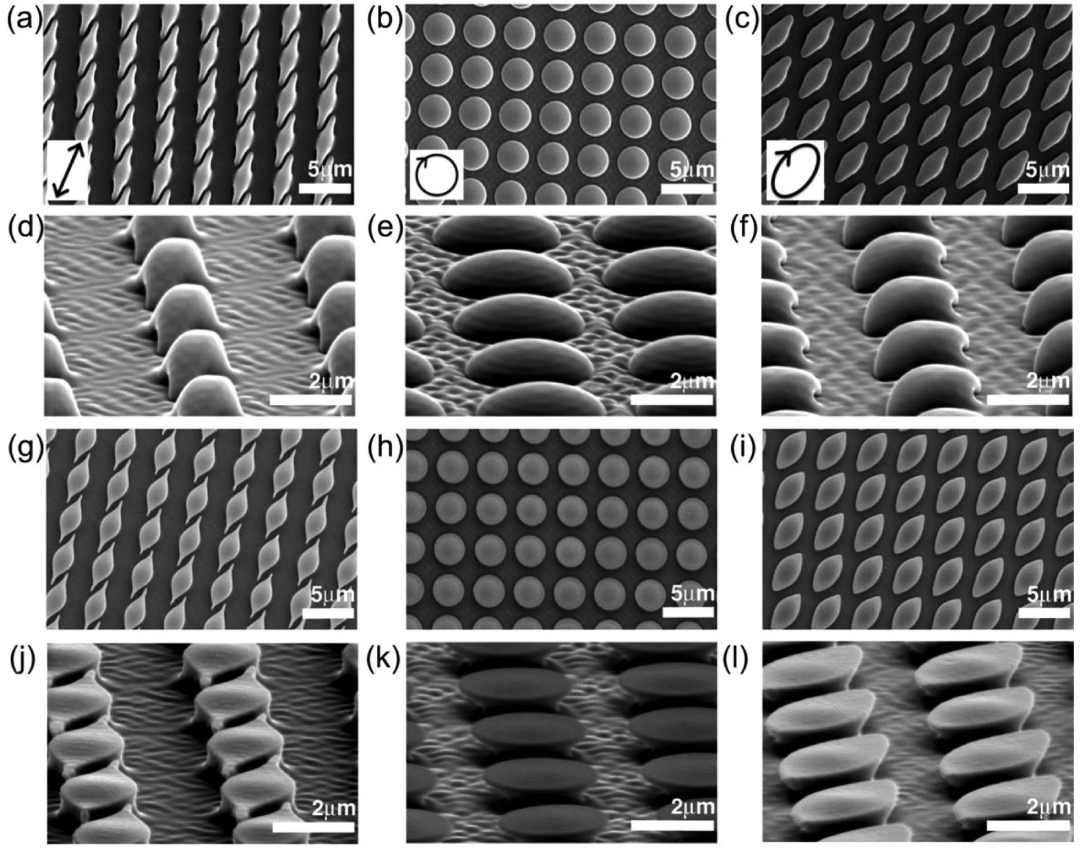


**Figure 2.** SEM images (top view) of the reshaped posts. (a) The light linear polarization direction is indicated by the arrow and is oriented along (a) the long axis of the reshaped structures (b) circularly, and (c) elliptically (short over long axis ratio of 0.5 (measured)). (d–f) Side views of structures shown in images a, b, and c, respectively. The polymer flows from the edges toward the substrate. (g–i) Top view of the reshaped posts in the case of PDMS capping layer for linearly, circularly, and elliptically polarized light. (j–l) Side view of the reshaped posts of panels g, h, and i. In the case of PDMS capping layer, the polymer adhesion to the PDMS prevents the material to flow to the substrate. All the structures have a flat top surface then, much similar to toroidal cavities. All the structures in this figure are obtained by exposing the samples to the expanded laser beam for 5 min with an intensity of 10 mW/cm$^2$.



DOI: 10.1021/acsami.5b01108
*ACS Appl. Mater. Interfaces* 2015, 7, 8209–8217

produced by means of standard soft imprinting onto a slide glass.[23,49] Each post is 2.0 $\mu$m in diameter and 1.6 $\mu$m in height. The periodicity in the array is of 4.0 $\mu$m (Figure 1a–c). After being prepared, the posts arrays were irradiated, following the illuminating scheme represented in Figure 1d,e. For this experiment, some of the samples were also covered with a transparent layer of PDMS 5 mm thick.

Laser beam parameters were then changed, resulting in different 3D structures. For this experiment, the laser beam (wavelength of 532 nm) with intensity of 30 mW/cm$^2$ was expanded and spatially filtered in order to obtain a large-area collimated beam (20 mm in diameter; Figure S3, Supporting Information). The laser polarization can be changed by use of waveplates, while the laser intensity was constant at 10 mW/cm$^2$ across the results in Figure 1–5. In the case of Figure 6, we used the Gaussian laser beam with intensity of 30 mW/cm$^2$. The exposure time was varied from 1 to 5 min.

In our first experiment, the laser beam was irradiated at normal incidence ($\theta$ = 0°) on a sample without the PDMS capping layer. The results of this exposure are shown in Figure 2 (the insets indicate the light polarization direction); we can clearly observe that the posts have been reshaped according to the light polarization. In particular, while the final shape of the posts after illumination with circularly polarized light still has a rotational symmetry, the shapes resulting from linear and elliptical polarization break the original symmetry of the pristine substrate. This effect is mainly due to the preferential direction in the glassy azo-polymer material displacement, parallel to the light polarization, while the long-axis of azobenzene molecules was found to be aligned in a direction perpendicular to the light polarization.[17] The schematic illustration of photofluidic movement of PDO3 along with azobenzene alignment state is presented in Figure S4 (Supporting Information). The perspective-view SEM images (Figure 2d–f) show that, for all polarization states, the material flow toward the edges of the posts, resulting into a fully 3D reshaping of the pristine structure. As nothing confines the light-driven mass-migration, the material can flow down to the residual layer on the substrate.

At this point, we repeated the experiment on the sample that includes a PDMS capping layer. In this case, the direction of the material flow is the same as without the extra PDMS capping layer (see top-view SEM images in Figure 2g–i). However, now, the adhesion between the PDO3 and PDMS is enough to keep the flowing azo-polymer always in contact with the PDMS capping layer. The final 3D features are then characterized by perspective-view SEM images for any of the polarization states (Figure 2j–l); no material flows down to the substrate, simply producing complex 3D shapes similar to toroidal microcavities (see more details in Figures S5 and S6, Supporting Information), the fabrication of which usually requires more sophisticated and expensive techniques. Moreover, this sophisticated 3D shaping can be achieved over a large area by single-step light illumination (Figure S7, Supporting Information).

The 3D structures obtained by these simple, single-step illumination schemes can be further tailored by changing the incident angle of the laser beam. In this case, in fact, the slanted projection of the beam on the pristine posts allows for further breaking the original symmetry. With illumination other than normal, the structures are elongated toward the beam incident direction. Figure 3 shows the results of slantwise illuminations at $\theta$ = 20° and $\theta$ = 40° with linearly polarized light in the case

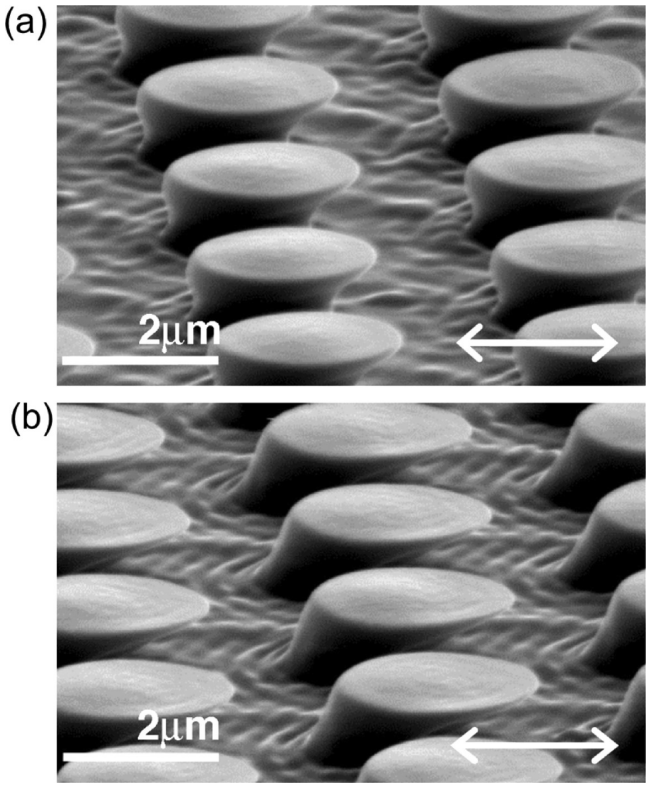


**Figure 3.** SEM image of reshaped posts obtained illuminating at an angle of (a) $\theta$ = 20° and (b) $\theta$ = 40° for 5 min a sample with PDMS capping layer. The white arrow indicates the light polarization direction. The structures are elongated toward the direction of the incident light.

of posts covered with a PDMS capping layer. In these conditions, due to the nonzero incidence angle, the cylindrical posts are not uniformly illuminated. Furthermore, as evident from FDTD simulations of light propagation through the pristine posts (Figure S8, Supporting Information), in our polymer, most of the light is absorbed in a superficial layer that is only a couple of hundreds nanometers thick (also see experimental demonstration of reshaping of 5.0 $\mu$m in diameter and 5.0 $\mu$m in height shown in Figure S9, Supporting Information).[23,49] This effect further increases the inhomogeneity in the case of slantwise illumination because part of each post is in the shadow and will contribute much less to the mass migration. As described later, the complex structures obtained by means of this simple illumination scheme allow producing anisotropic hydrophobic substrates.

We develop here a preliminary modeling of the light-induced reshaping process with the main purpose of demonstrating that this process is indeed deterministic and predictable. Our model catches some of the main qualitative features of the light-induced mass migration process. Let us consider a single cylinder of light-sensitive azo-material standing on a plane substrate. We choose the coordinate system so as to have the $xy$ plane coincident with the substrate surface and the $z$ axis along the cylinder axis (Figure S10, Supporting Information). To simplify the problem, we shall focus here only on the dynamical reshaping of the lateral surface of the cylinder occurring under illumination by a linearly polarized plane wave impinging at normal incidence. We describe this lateral surface as a 2D closed curve in the $xy$ plane, corresponding to the contour of the top surface of a post, which can be defined parametrically


DOI: 10.1021/acsami.5b01108
ACS Appl. Mater. Interfaces 2015, 7, 8209–8217

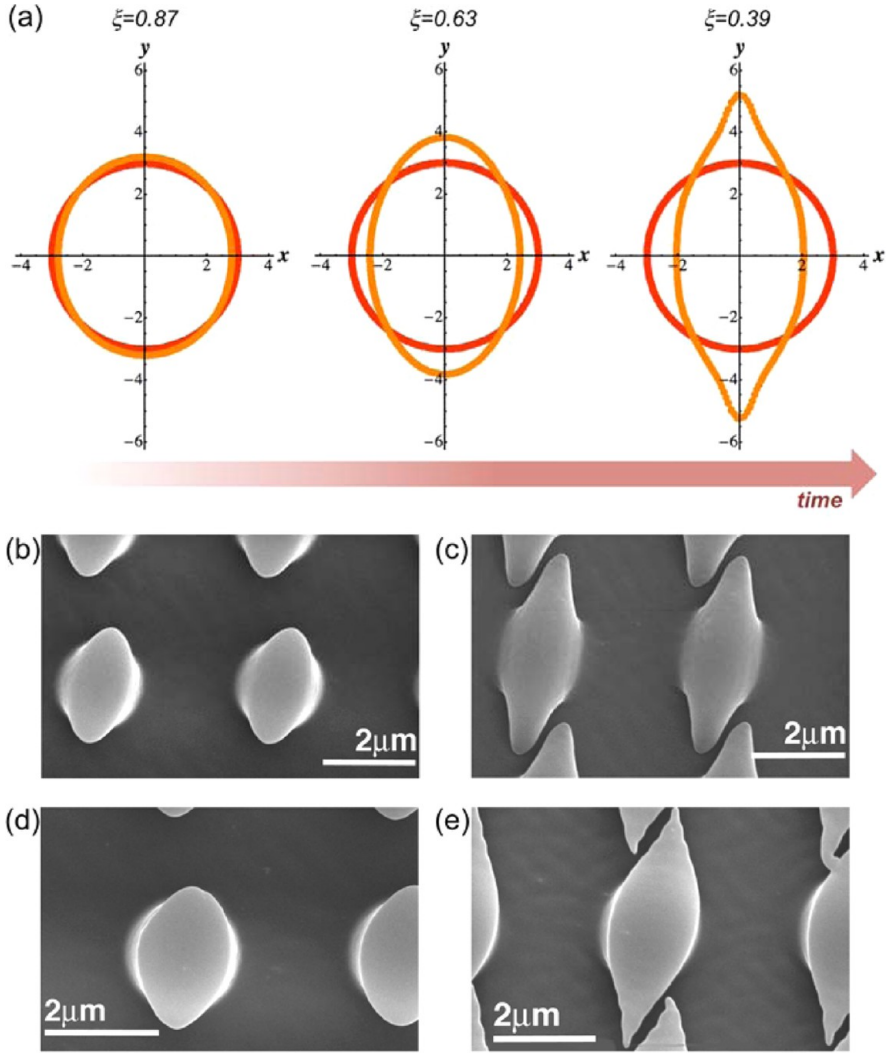


**Figure 4.** (a) Three steps of the time evolution predicted by our phenomenological model for the reshaping of the azo-posts under illumination with light that is linearly polarized along the *y* axis. The red circle represents the contour of the pristine post top surface. The orange lines represent the new contour after reshaping. The two steps on the side correspond to a ratio ($\xi$) between the short and long axes of the reshaped structures of 0.63 and 0.39. These are found experimentally to correspond to exposure times of 3 and 5 min, respectively. The results of illuminating for such time intervals are shown by SEM pictures without PDMS capping layer for (b) 3 min and (c) 5 min and with PDMS capping layer for (d) 3 min and (e) 5 min. During illumination, the light is linearly polarized along the long axes of the reshaped structures.

by the two functions $x(s)$ and $y(s)$, where $s$ is an arbitrary continuous parameter (Figure S10, Supporting Information). We take $s$ to belong to the fixed range $[0,1]$, so that the curve closure corresponds to the periodicity conditions $x(0) = x(1)$ and $y(0) = y(1)$. During the irradiation, the curve is also a function of time $t$, so that $x(s,t)$ and $y(s,t)$ will actually be functions of two independent variables, $s$ and $t$. At the initial time $t = 0$, when the irradiation starts, the curve is taken to be a circle, as given by below two equations:

$$x(s) = r\cos(2\pi s) \tag{1}$$

$$y(s) = r\sin(2\pi s) \tag{2}$$

In above equations, the $r$ indicates the radius of cylinder. It will be also useful to introduce the normal and tangential directions at any given point on the curve, as indicated by the unit vectors $\boldsymbol{n}$ and $\boldsymbol{t}$ shown in Figure S10, Supporting Information. For the light-induced mass current, we adopt here the phenomenological model demonstrated in our previous report.[20,22] The optical electric field due to the impinging plane wave can be considered uniform, to first approximation, neglecting the effects of the dielectric cylinder on the wave itself. Then, all mass-current terms arising from optical gradients vanish, and we are left only with the boundary current given by the following expression:

$$J_t = \frac{C_B}{L}(E_n^* E_t + \text{cc}) \tag{3}$$

where $J_t$ denotes the tangential component of the mass current (the normal component is assumed to vanish), $C_B$ is a characteristic coefficient of the azopolymer response, $L$ is an effective penetration length in the polymer (as we will see this quantity will cancel in the final expressions), $E_n^*$ and $E_t$ are the normal and tangential electric field components at each point on the surface, and cc denotes the complex conjugate term.

Now, the surface reconfiguration for a short time interval can be calculated as a local displacement $\Delta h(s)$ along the curve normal direction (in the $xy$ plane) resulting from the mass inflow or outflow due to the surface mass current, which is


DOI: 10.1021/acsami.5b01108
ACS Appl. Mater. Interfaces 2015, 7, 8209−8217

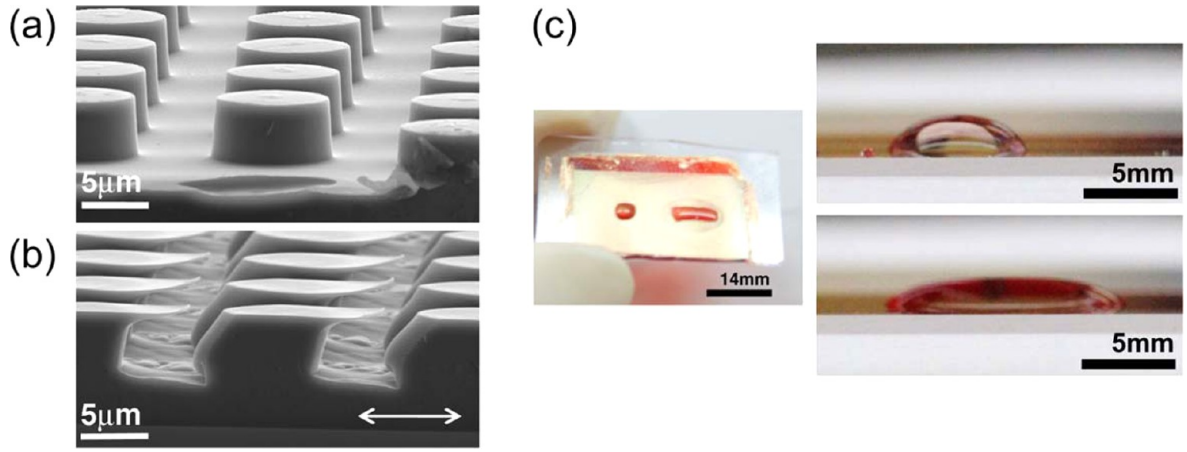


**Figure 5.** (a) SEM image of pristine PDO3 posts array (10 $\mu$m diameter, 10 $\mu$m height, 20 $\mu$m periodicity). (b) Reshaped posts after illumination (10 mW/cm$^2$ for 10 min) with the expanded, linearly polarized, laser beam incident at $\theta = 60°$. The white arrow represents the light polarization direction. (c) Picture of the effect of structures shown in panels a and b on colored water droplets. The pristine posts have almost no effect on the droplet, while the reshaped posts force the droplet to be elongated in the same direction of the structures bending.

tangential to the curve. Assuming (approximate) incompressibility of the azo-PDO3, this variation can be linked to the mass-current via the continuity equation, with the following result:

$$\frac{\partial h}{\partial t}(s) = -\left(\frac{L}{\rho}\right)\frac{\partial J_t}{\partial l_t} = -\left(\frac{L}{\rho}\right)\frac{1}{\sqrt{\left(\frac{\partial x}{\partial s}\right)^2 + \left(\frac{\partial y}{\partial s}\right)^2}}\frac{\partial J_t}{\partial s} \tag{4}$$

where we denoted as $l_t$ the (local) curve length along the tangential direction. To make these expressions explicit, we only need to compute the derivative of the mass current with respect to the curve parameter $s$. The explicit result and the corresponding evolution equations for the functions $x(s,t)$ and $y(s,t)$ are given in the Supporting Information. A term describing a surface tension was also included in the complete model. On inspection of the dynamical equations, it is evident that the PDO3 surface at a given time will undergo a deformation only in those locations in which the surface is not flat, as quantified by a nonzero second derivative of the curve functions. This shows a key point of our results because the nonuniform light distributions that are usually exploited to modulate the flat surface of azo-material films in complex shapes are replaced here with pristine 3D shapes that allow coupling a non uniform surface to a "flat" optical field.

The evolution equations were solved numerically by a standard finite-difference Lax method, although the solution had to be always limited in total integration time as a form of high-frequency numerical instability eventually dominated the results for longer times. Figure 4a shows three intermediate steps of the calculated time sequence of the structural evolution driven by the irradiation of linearly polarized light (along $y$ axis) on the PDO3 cylinder posts. The coefficient $\xi$ is the ratio between the short and long axes of the reshaped post (the axis units are arbitrary). These values are fully consistent with the experimental counterparts presented in Figure 4b−c (illumination without PDMS capping layer) and Figure 4d−e (illumination with PDMS capping layer) resulting from 3 min (panels b and d) and 5 min (panels c and e) of exposure to the illuminating beam.

Control of fluidic wetting offers a route to wide scientific and technological implications for fields ranging from 3D fabrication of micro- and nanoarchitectures and bioinspired superhydrophobic surfaces to microfluidic lab-on-a-chip systems.[51−55] Our arrays of reshaped 3D azo-material posts can be, for example, used to directionally change the wetting behavior of surfaces.[56] An example is shown in Figure 5a−c. An array of pristine posts (each post is 10.0 $\mu$m in diameter and 9.0 $\mu$m in height, as shown in Figure 5a) covered with a PDMS capping layer has been illuminated with linearly polarized light incident at $\theta = 60°$. The result of this illumination is shown in Figure 5b; as with the result in Figure 3, the initially symmetric cylinder was reconfigured into the 3D asymmetric shapes. Figure 5c shows a digital image of a substrate where both pristine and reshaped posts are present, simultaneously; two drops of colored water (red colored surfactant Triton X-100 was dispersed in deionized water with 0.2 wt %) with 2 $\mu$L volume were deposited onto the pristine (left) and reconfigured (right) area. The isotropic spreading of the water droplet was clearly observed onto the pristine arrays, whereas the area of the reconfigured array elucidated the anisotropic, unidirectional water droplet spreading that results from reshaping at slantwise illumination. The side-view macroscopic images in the right panel of Figure 5c showed a far more significant impact of asymmetric feature on unidirectional wetting. As anticipated based on such 3D controlled asymmetric structure, the local energy to pin the liquid was induced in less than one direction; consequently, at least, asymmetric factor of 2−2.5 (ratio of short axis to long axis of elongated water droplet) was achieved in our methods. It is worth noting that our 3D structuring is only limited to the illuminated area, with no changes of other areas on the sample, as instead observed for other techniques such as heat-induced or electro-hydrodynamic forces. This could allow producing engineered hydrophobic surfaces with a prescribed map of local anisotropy and directionality in the wetting properties.

Another application that demonstrates the potential of our 3D shaping approach is the realization of micro- and nanochannels for molecular sensing and filtering. The latter has recently gained consensus as a valid technique in filtering long, polymer-like, molecules such as DNA; but, unfortunately, much of the previous works focused on complicated and expensive processes (e.g., electron beam lithography and focused ion beam lithography).[57] In our approach, we applied the one-step photofluidic reconfiguration of a pristine azo-


DOI: 10.1021/acsami.5b01108
ACS Appl. Mater. Interfaces 2015, 7, 8209−8217

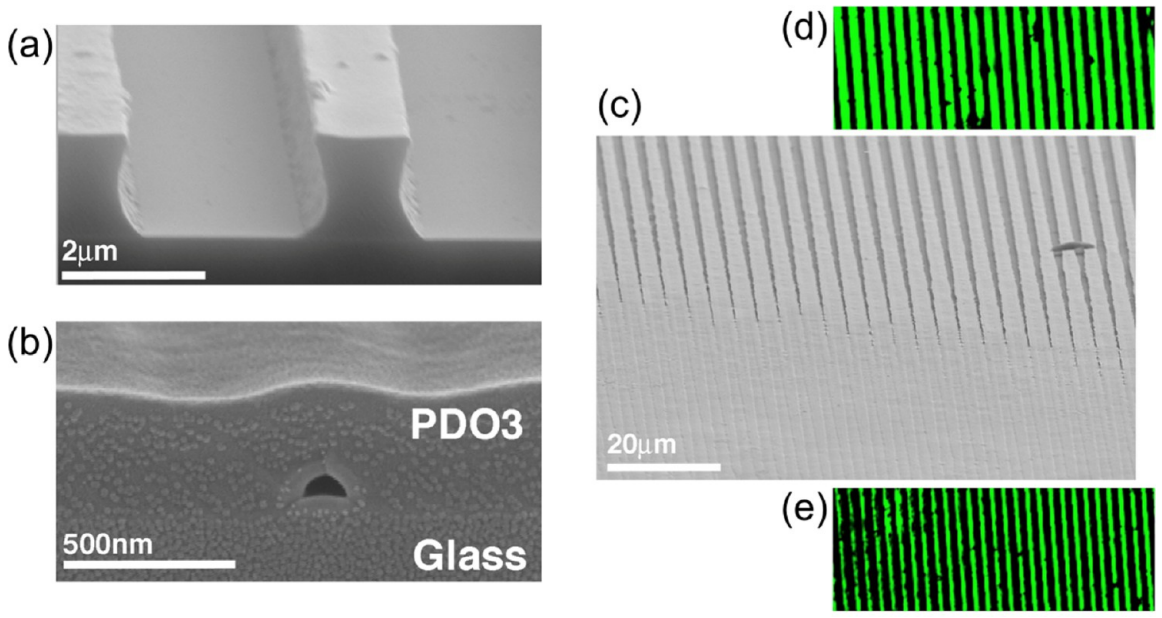


**Figure 6.** (a) SEM image of the PDO3 grating. Each groove is 1.2 $\mu$m wide and 2 $\mu$m high. The grating has a 4 $\mu$m periodicity. (b) View of the minimum feature size obtained at the edge of the grating after illumination with linearly polarized light perpendicularly to the grooves. The polymer flow causes the narrowing of the channels between the grooves, but the channels do not close completely due to the presence of a PDMS capping layer during illumination. The laser beam was not expanded and spatially filtered, thus keeping its original Gaussian shape that is used to impose a gradient in the amount of closure of the channels in a one-step illumination. This is evident in (c) the SEM image of the grooves after illumination when the center of the Gaussian beam is located at the lower edge of the grating. (d) Optical fluorescence image of the channels in the (d) upper and (e) lower parts of the reshaped grating while the dye Lucifer yellow in water is flowing in the channels.

material structure, to the simple and cost-effective fabrication of complex micro- and nanochannels. Toward this direction, we started from a grating of PDO3 whose grooves are 1.2 $\mu$m width, with a periodicity of 4 $\mu$m (Figure 6a). The pristine PDO3 arrays were developed on glass substrates by micromolding in capillary (MIMIC)[11,13] with custom built translational stage[50] and then covered with a PDMS capping layer. In this configuration, the illuminating laser beam was used without any spatial filtering, resulting in a beam with a Gaussian profiled intensity and an average intensity on the sample surface of 30 mW/cm$^2$. The beam illuminates the sample at normal incidence for 5 min, linearly polarized in the direction perpendicular to the grooves. The result of such illumination is shown in Figure 6b,c. In particular, Figure 6c shows the top-view SEM image of the illuminated sample. It is clear that the size of the pristine channels is now reduced by effect of the photoinduced flow of the azo-PDO3 along the light polarization direction. Furthermore, the degree of size reduction of the channels follows the Gaussian profile of the illuminating beam, thus producing much narrower channels where the local laser intensity is higher (beam center). This result indicates that the development of the funnel-shaped entrance of micro- and nanofluidic channel, which has been long-standing challenge in the relevant field,[57] can be achieved in a more versatile way. Figure 6b further clarifies some characteristic of the process. The channels do not close completely during the mass flow thanks to the adhesion to the PDMS capping layer. The final dimensions achieved with this fabrication method are easily smaller than 100 nm in diameter: in our experimental conditions, minimum feature size of 30 nm in lateral and height of nanochannel has been reliably achieved (Figure S11, Supporting Information). To highlight the structural features of the obtained fluidic channels, we loaded Lucifer yellow dye (2 wt %), dissolved in water into the reshaped PDO3 fluidic channels; the dye-loaded water was injected into the fluidic channel by means of capillarity. Figure 6d,e shows the fluorescence optical microscope images of the top and bottom part of Figure 6c after the dye-loaded water has been injected, enabling us to track water flow within the developed micro- and nanochannel. From the fluorescence optical microscope image, we did not observe any significant leaks in the channel; these data indicate that the monolithic PDO3 fluidic channel can work very well.

## CONCLUSIONS

The experiments described above prove once again the peculiar characteristics of azobenzene-containing polymers in terms of micro- and nanofabrications. A standard photoresist responds to the illuminating light by means of a photoconversion that reflects the incident light intensity pattern. Azo-based polymers instead respond to both the light intensity and the light polarization status. In particular, here, we show that even a completely flat optical field, a plane wave, can originate complex structures if coupled to some geometrical characteristics of prepatterned films of azo-polymers. This behavior is fully demonstrated by our model, in which all the nonzero terms in the mathematical description of the material-flow are due to the coupling of a nonuniform surface to a uniform optical field. In fact, although the incident field could be modified by the 3D pristine structures, we found that this effect is negligible in the surface area (see FDTD simulations in Figure S8, Supporting Information). In our phenomenological model, there is no contribution from optical gradients. The mass flow only originates from the coupling of the uniform optical field to the time-changing curved contour of the post that provides nonzero derivatives in the mathematical description.

Although the experimental part in our new 3D structuring schemes is quite simple regarding both the preparation of the


DOI: 10.1021/acsami.5b01108
ACS Appl. Mater. Interfaces 2015, 7, 8209−8217

sample and the exposure to light, the complexity of the three-dimensional structures obtained is comparable to those obtained with more complicated (and expensive) methods based on electron beam lithography. Finally, the anisotropic hydrophobic surfaces and funnel-shaped nanochannels that we presented here are two typical examples of the practical devices that may be produced by using our new approach, adding new functionalities in cheap and easily produced substrates for microfluidic and biological applications.

## ■ ASSOCIATED CONTENT

### Supporting Information

Characteristics of PDO3 (chemical structure and absorption spectrum of PDO3), schematic illustration of laser setup, schematic portraits of azobenzene alignment state during photofluidization, SEM and OM image of structure evolution of PDO3 post arrays after light irradiation, detailed description of the phenomenological modeling, and cross-sectional SEM images of nanofluidic channel. This material is available free of charge via the Internet at http://pubs.acs.org.

## ■ AUTHOR INFORMATION

### Corresponding Authors

*E-mail: seungwoo@skku.edu. Web: http://seungwoo.skku.edu.

*E-mail: antonio.ambrosio@ cnr.it.

### Author Contributions

S.L. conceived the original idea. S.L. and H.S.K. designed and conducted the experiments. A.A. and L.M. developed the phenomenological model and performed numerical calculations. S.L. performed FDTD numerical computation. S.L., A.A., and L.M. wrote the paper. All the authors discussed the data and commented on the paper. All authors have given approval to the final version of the manuscript. S.L. H.S.K. and A.A. equally contributed to this work.

### Notes

The authors declare no competing financial interest.

## ■ ACKNOWLEDGMENTS

This work was supported by Samsung Scholarship Research Fund 2014 program at Sungkyunkwan University (No. S-2014-0883- 000) and the Pioneering Nano-Based Convergence HRD Center (BK21+ program at Sungkyunkwan University), the Basic Science Research Program (2009-0083540) of the National Research Foundation of Korea (NRF) funded by the Ministry of Education, Science, and Technology, Korea (the 8th National Core Research Center at Sungkyunkwan University, named by Center for Human Interface Nano Technology, HINT).

## ■ REFERENCES

(1) Scaffer, E.; Thurn-Albrecht, T.; Russell, T. P.; Steiner, U. Electrically Induced Structure Formation and Pattern Transfer. *Nature* **2000**, *403*, 874−877.

(2) Morariu, M. D.; Voicu, N. E.; Schäffer, E.; Lin, Z.; Russell, T. P.; Steiner, U. Hierarchical Structure Formation and Pattern Replication Induced by an Electric Field. *Nat. Mater.* **2002**, *2*, 48−52.

(3) Verma, R.; Sharma, A.; Kargupta, K.; Bhaumik, J. Electric Field Induced Instability and Pattern Formation in Thin Liquid Films. *Langmuir* **2005**, *21*, 3710−3721.

(4) Collins, R. T.; Jones, J. J.; Harris, M. T.; Basaran, O. A. Electrohydrodynamic Tip Streaming and Emission of Charged Drops from Liquid Cones. *Nat. Phys.* **2007**, *4*, 149−154.

(5) Chou, S. Y.; Xia, Q. Improved Nanofabrication through Guided Transient Liquefaction. *Nat. Nanotechnol.* **2008**, *3*, 295−300.

(6) Wang, Y.; Liang, X.; Liang, Y.; Chou, S. Y. Sub-10-nm Wide Trench, Line, and Hole Fabrication Using Pressed Self-Perfection. *Nano Lett.* **2008**, *8*, 1986−1990.

(7) Ferraro, P.; Coppola, S.; Grilli, S.; Paturzo, M.; Vespini, V. Dispensing Nano−Pico Droplets and Liquid Patterning by Pyroelectrodynamic Shooting. *Nat. Nanotechnol.* **2010**, *5*, 429−435.

(8) Bhat, P. P.; Appathurai, S.; Harris, M. T.; Pasquali, M.; McKinley, G. H.; Basaran, O. A. Formation of Beads-on-a-String Structures during Break-up of Viscoelastic Filaments. *Nat. Phys.* **2010**, *6*, 625−631.

(9) Grilli, S.; Coppola, S.; Vespini, V.; Merola, F.; Finizio, A.; Ferraro, P. 3D Lithography by Rapid Curing of the Liquid Instabilities at Nanoscale. *Proc. Natl. Acad. Sci. U.S.A.* **2011**, *108*, 5106−15111.

(10) Zheng, Y.; Bai, H.; Huang, Z.; Tian, X.; Nie, F.-Q.; Zhao, Y.; Zhai, J.; Jiang, L. Directional Water Collection on Wetted Spider Silk. *Nature* **2010**, *463*, 640−643.

(11) Lee, S.; Shin, J.; Lee, Y.-H.; Fan, S.; Park, J.-K. Directional Photofluidization Lithography for Nanoarchitectures with Controlled Shapes and Sizes. *Nano Lett.* **2010**, *10*, 296−304.

(12) Yu, H.; Ikeda, T. Photocontrollable Liquid-Crystalline Actuators. *Adv. Mater.* **2011**, *23*, 2149−2180.

(13) Lee, S.; Shin, J.; Lee, Y.-H.; Park, J.-K. Fabrication of the Funnel-Shaped Three-Dimensional Plasmonic Tip Arrays by Directional Photofluidization Lithography. *ACS Nano* **2010**, *4*, 7175−7184.

(14) Viswanathan, N. K.; Kim, D. Y.; Bian, S.; Williams, J.; Liu, W.; Li, L.; Samuelson, L.; Kumar, J.; Tripathy, S. K. Surface Relief Structures on Azo Polymer Films. *J. Mater. Chem.* **1999**, *9*, 1941−1955.

(15) Natansohn, A.; Rochon, P. Photoinduced Motions in Azo-Containing Polymers. *Chem. Rev.* **2002**, *102*, 4139−4175.

(16) Karageorgiev, P.; Neher, D.; Schulz, B.; Stiller, B.; Pietsch, U.; Giersig, M.; Brehmer, L. From Anisotropic Photo-fluidity towards Nanomanipulation in the Optical Near-field. *Nat. Mater.* **2005**, *4*, 699−703.

(17) Lee, S.; Kang, H. S.; Park, J.-K. High-Resolution Patterning of Various Large-Area, Highly Ordered Structural Motifs by Directional Photofluidization Lithography: Sub-30-nm Line, Ellipsoid, Rectangle, and Circle Arrays. *Adv. Funct. Mater.* **2011**, *21*, 1770−1778.

(18) Yu, H. Recent Advances in Photoresponsive Liquid-crystalline Polymers Containing Azobenzene Chromophores. *J. Mater. Chem. C* **2014**, *2*, 3047−3054.

(19) Lee, S.; Kang, H. S.; Park, J.-K. Directional Photofluidization Lithography: Micro/Nanostructural Evolution by Photofluidic Motions of Azobenzene Materials. *Adv. Mater.* **2012**, *24*, 2069−2103.

(20) Ambrosio, A.; Marrucci, L.; Borbone, F.; Roviello, A.; Maddalena, P. Light-Induced Spiral Mass Transport in Azo-Polymer Films under Vortex-Beam Illumination. *Nat. Commun.* **2012**, *3*, 989.

(21) Fang, G. J.; Maclennan, J. E.; Yi, Y.; Glaser, M. A.; Farrow, M.; Korblova, E.; Walba, D. M.; Furtak, T. E.; Clark, N. A. Athermal Photofluidization of Glasses. *Nat. Commun.* **2013**, *4*, 1521.

(22) Ambrosio, A.; Maddalena, P.; Marrucci, L. Molecular Model for Light-Driven Spiral Mass Transport in Azopolymer Films. *Phys. Rev. Lett.* **2013**, *110*, 146102.

(23) Lee, S.-A.; Kang, H. S.; Park, J.-K.; Lee, S. Vertically Oriented, Three-Dimensionally Tapered Deep-Subwavelength Metallic Nanohole Arrays Developed by Photofluidization Lithography. *Adv. Mater.* **2014**, *25*, 7521−7528.

(24) Priimagi, A.; Shevchenko, A. Azopolymer-based Micro- and Nanopatterning for Photonic Applications. *J. Polym. Sci., Part B: Polym. Phys.* **2014**, *52*, 163−182.

(25) Priimagi, A.; Barrett, C. J.; Shishido, A. Recent Twists in Photoactuation and Photoalignment Control. *J. Mater. Chem. C* **2014**, *2*, 7155−7162.

(26) Kang, H. S.; Kim, H.-T.; Park, J.-K.; Lee, S. Light-Powered Healing of a Wearable Electrical Conductor. *Adv. Funct. Mater.* **2014**, *24*, 7273−7283.



DOI: 10.1021/acsami.5b01108
*ACS Appl. Mater. Interfaces* 2015, 7, 8209−8217

(27) Kim, D. Y.; Tripathy, S. K.; Li, L.; Kumar, J. Laser-induced Holographic Surface Relief Gratings on Nonlinear Optical Polymer Films. *Appl. Phys. Lett.* **1995**, *66*, 1166−1168.
(28) Kim, D. Y.; Li, L.; Jiang, X. L.; Shivshankar, V.; Kumar, J.; Tripathy, S. K. Polarized Laser Induced Holographic Surface Relief Gratings on Polymer Films. *Macromolecules* **1995**, *28*, 8835−8839.
(29) Bian, S.; Williams, J. M.; Kim, D. Y.; Li, L.; Balasubramanian, S.; Kumar, J.; Tripathy, S. Photoinduced Surface Deformations on Azobenzene Polymer Films. *J. Appl. Phys.* **1999**, *86*, 4498−4508.
(30) Barrett, C. J.; Natansohn, A. L. Mechanism of Optically Inscribed High-Efficiency Diffraction Gratings in Azo Polymer Films. *J. Phys. Chem.* **1996**, *100*, 8836−8842.
(31) Barret, C. J.; Rochon, P. L.; Natansohn, A. L. Model of Laser-Driven Mass Transport in Thin Films of Dye-Functionalized Polymers. *J. Chem. Phys.* **1998**, *109*, 1505−1516.
(32) Lefin, P.; Fiorini, C.; Nunzi, J.-M. Anisotropy of the Photo-Induced Translation Diffusion of Azobenzene Dyes in Polymer Matrices. *Pure Appl. Opt.* **1998**, *7*, 71−82.
(33) Kumar, J.; Li, L.; Jiang, X. L.; Kim, D.-Y.; Lee, T. S.; Tripathy, S. Gradient Force: The Mechanism for Surface Relief Grating Formation in Azobenzene Functionalized Polymers. *Appl. Phys. Lett.* **1998**, *72*, 2096−2098.
(34) Pedersen, T. G.; Johansen, P. M.; Holme, N. C. R.; Ramanujam, P. S.; Hvilsted, S. Mean-Field Theory of Photoinduced Formation of Surface Reliefs in Side-Chain Azobenzene Polymers. *Phys. Rev. Lett.* **1998**, *80*, 89−92.
(35) Toshchevikov, V.; Saphiannikova, M.; Heinrich, G. Microscopic Theory of Light-Induced Deformation in Amorphous Side-Chain Azobenzene Polymers. *J. Phys. Chem. B* **2009**, *113*, 5032−5045.
(36) Bublitz, D.; Fleck, B.; Wenke, L. A Model for Surface-relief Formation in Azobenzene Polymers. *Appl. Phys. B: Laser Opt.* **2001**, *72*, 931−936.
(37) Ambrosio, A.; Camposeo, A.; Carella, A.; Borbone, F.; Pisignano, D.; Roviello, A.; Maddalena, P. Realization of Submicrometer Structures by a Confocal System on Azopolymer Films Containing Photoluminescent Chromophores. *J. Appl. Phys.* **2010**, *107*, 083110.
(38) Ambrosio, A.; Maddalena, P.; Carella, A.; Borbone, F.; Roviello, A.; Polo, M.; Neves, A. A. R.; Camposeo, A.; Pisignano, D. Two-Photon Induced Self-Structuring of Polymeric Films Based on Y-Shape Azobenzene Chromophore. *J. Phys. Chem. C* **2011**, *115*, 13566−13570.
(39) Weigert, F. Dichroism Induced in a Fine-Grain Silverchloride Emulsion by a Beam of Linearly Polarized Light. *Verh. Dtsch. Phys. Ges.* **1919**, *21*, 479−483.
(40) Yager, K. G.; Barrett, C. J. Novel Photo-Switching using Azobenzene Functional Materials. *J. Photochem. Photobiol., A* **2006**, *182*, 250−261.
(41) Yu, H.; Kobayashi, T. Photoresponsive Block Copolymers Containing Azobenzenes and Other Chromophores. *Molecules* **2010**, *15*, 570−603.
(42) Lee, S.; Jeong, Y.-C.; Park, J.-K. Facile Fabrication of Close-Packed Microlens Arrays using Photoinduced Surface Relief Structures as Templates. *Opt. Express* **2007**, *15*, 14550−14559.
(43) Lee, S.; Jeong, Y.-C.; Park, J.-K. Unusual Surface Reliefs from Photoinduced Creeping and Aggregation Behavior of Azopolymer. *Appl. Phys. Lett.* **2008**, *93*, 031912.
(44) Ambrosio, A.; Camposeo, A.; Maddalena, P.; Patanè, S.; Allegrini, M. Real-Time Monitoring of the Surface Relief Formation on Azo-Polymer Films upon near-Field Excitation. *J. Microsc.* **2008**, *229*, 307−312.
(45) Kang, H. S.; Lee, S.; Park, J.-K. Monolithic, Hierarchical Surface Reliefs by Holographic Photofluidization of Azopolymer Arrays: Direct Visualization of Polymeric Flows. *Adv. Funct. Mater.* **2011**, *21*, 4412−4422.
(46) Kravchenko, A.; Shevchenko, A.; Ovchinnikov, V.; Priimagi, A.; Kaivola, M. Optical Interference Lithography Using Azobenzene-Functionalized Polymers for Micro- and Nanopatterning of Silicon. *Adv. Mater.* **2011**, *23*, 4174−4177.
(47) Lee, S.; Shin, J.; Kang, H. S.; Lee, Y.-H.; Park, J.-K. Deterministic Nanotexturing by Directional Photofluidization Lithography. *Adv. Mater.* **2011**, *23*, 3244−3250.
(48) Koskela, J. E.; Liljeström, V.; Lim, J.; Simanek, E. E.; Ras, R. H. A.; Priimagi, A.; Kostiainen, M. A. Light-Fuelled Transport of Large Dendrimers and Proteins. *J. Am. Chem. Soc.* **2014**, *136*, 6850−6853.
(49) Kang, H. S.; Lee, S.; Lee, S.-A.; Park, J.-K. Multi-Level Micro/Nanotexturing by Three-Dimensionally Controlled Photofluidization and its Use in Plasmonic Applications. *Adv. Mater.* **2013**, *25*, 5490−5497.
(50) Lee, S.; Kim, S.; Kim, T.-T.; Kim, Y.; Choi, M.; Lee, S. H.; Kim, J.-Y.; Min, B. Reversibly Stretchable and Tunable Terahertz Metamaterials with Wrinkled Layouts. *Adv. Mater.* **2012**, *24*, 3491−3497.
(51) Choi, C.-H.; Lee, J.; Yoon, K.; Tripathy, A.; Stone, H. A.; Weitz, D. A.; Lee, C.-S. Surface-Tension-Induced Synthesis of Complex Particles Using Confined Polymeric Fluids. *Angew. Chem., Int. Ed.* **2010**, *49*, 7748−7752.
(52) Sacanna, S.; Korpics, M.; Rodriguez, K.; Colón-Meléndez, L.; Kim, S.-H.; Pine, D. J.; Yi, G.-R. Shaping Colloids for Self-Assembly. *Nat. Commun.* **2013**, *4*, 1688.
(53) Erbil, H. Y.; Demirel, A. L.; Avci, Y.; Mert, O. Transformation of a Simple Plastic into a Superhydrophobic Surface. *Science* **2003**, *299*, 1377−1380.
(54) Li, X.-M.; Reinhoudt, D.; Crego-Calama, M. What Do We Need for a Superhydrophobic Surface? A Review on the Recent Progress in the Preparation of Superhydrophobic Surfaces. *Chem. Soc. Rev.* **2006**, *36*, 1350−1368.
(55) Cho, S. K.; Moon, H.; Kim, C. J. Creating, Transporting, Cutting, and Merging Liquid Droplets by Electrowetting-based Actuation for Digital Microfluidic Circuits. *J. Microelectromech. Syst.* **2003**, *12*, 70−80.
(56) Chu, K.-H.; Xiao, R.; Wang, E. N. Uni-directional Liquid Spreading on Asymmetric Nanostructured Surfaces. *Nat. Mater.* **2010**, *9*, 413−417.
(57) Chantiwas, R.; Park, S.; Soper, S. A.; Kim, B. C.; Takayama, S.; Sunkara, V.; Hwang, H.; Cho, Y.-K. Flexible Fabrication and Applications of Polymer Nanochannels and Nanoslits. *Chem. Soc. Rev.* **2011**, *40*, 3677−3702.


DOI: 10.1021/acsami.5b01108
*ACS Appl. Mater. Interfaces* 2015, 7, 8209−8217